Quantization of Filter Bank Frame Expansions Through Moving Horizon Optimization

Daniel E. Quevedo, *Member, IEEE*, Helmut Bölcskei, *Fellow, IEEE*, and Graham C. Goodwin, *Fellow, IEEE*

***Abstract*—This paper describes a novel approach to quantization in oversampled filter banks. The new technique is based on moving horizon optimization, does not rely on an additive white noise quantization model and allows stability to be explicitly enforced in the associated nonlinear feedback loop. Moreover, the quantization structure proposed here includes $\Sigma\Delta$ and linear predictive subband quantizers as a special case and, in general, outperforms them.**

***Index Terms*—Filter banks, frame expansions, oversampling, quantization.**

I. Introduction

FILTERBANKS (FBs) are widespread in many practical applications, mainly in relation to subband signal processing and coding of audio and image signals; see, e.g., [1]–[7]. Fig. 1 depicts a FB with K-channels and decimation factor L in each channel, where $K \geq L$. The FB is said to be *critically sampled* if $K = L$ and *oversampled* if $K > L$. The main purpose of a critically sampled FB is to compress a discrete-time input signal y into sequences u_i, such that the number of bits used to quantize the subband signals v_i is small, whilst providing "good" reconstruction quality, i.e., while achieving $\hat{y} \approx y$. For that purpose, a series connection of an *analysis FB*, an abstract *quantizer* (or coder) $\mathcal{Q}$ and a *synthesis FB* is employed.

As can be seen in Fig. 1, a FB first decomposes the discrete-time input signal y into subband sequences v_i through analysis filtering and downsampling. The abstract quantizer $\mathcal{Q}$ then processes the resulting K subband sequences (in a linear or nonlinear fashion) and quantizes them, giving rise to the output sequences u_i. Finally, the synthesis FB upsamples and filters the sequences u_i to provide an estimate of y.

Reconstruction errors in a FB basically arise from three sources [3]: aliasing and imaging (as a consequence of sampling rate conversions), phase and amplitude distortion (due to the filters employed), and quantization effects. The effects of aliasing, imaging, phase and amplitude distortion can be dealt with by proper design of the analysis and the synthesis filters; see, e.g., [3]–[5]. On the other hand, quantization, in general, incurs a loss of information, and, therefore, precludes $\hat{y}$ from being equal to y. Quantization effects are nonlinear (and nonsmooth) in nature. Nonetheless, often linear analysis and design methodologies can usefully be employed; see, e.g., [8]–[11]. Of course, these techniques are only approximate and one can expect linear design approaches to be, in general, outperformed by nonlinear ones.

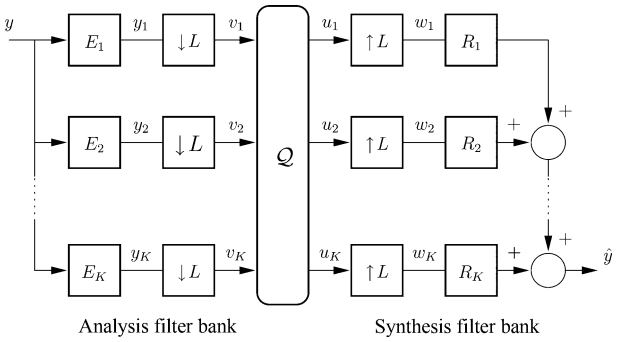

Fig. 1. K-channel filter bank with decimation factor L.

While source coding applications typically employ critically sampled FBs, oversampled FBs implement redundant signal expansions in $\ell^2(\mathbb{Z})$ and have inherent noise reducing properties rendering them attractive for applications requiring low-resolution quantizers. In the context of analog-to-digital (A/D) conversion, the practical advantages of using low-resolution quantizers at the cost of increased (sampling) rate are indicated by the popular $\Sigma\Delta$ techniques [12], [13]. The use of low-resolution quantizers increases circuit speed and reduces circuit complexity; 1-bit codewords, for example, eliminate the need for word framing.

In [8], oversampling noise shaping $(\Sigma\Delta)$ subband quantizers have been introduced as an extension of oversampled noise shaping A/D converters. The approach in [8] has two shortcomings:

1) a linear model for quantization is used, i.e., quantization is modeled as introducing additive white noise independent of the signal, and
2) stability of the feedback loop cannot be guaranteed.

In the present paper, we address these two issues by introducing a novel quantization method for oversampled FBs. The approach uses an exact nonlinear model of quantization and allows one to enforce stability. The new scheme is based on ideas from finite-set constrained predictive control; see, e.g., [14]. On

Manuscript received November 23, 2007; revised September 05, 2008. First published October 31, 2008; current version published January 30, 2009. This paper was presented in part at the 43rd IEEE Conference on Decision and Control,Paradise Island, Bahamas, December 2004. The associate editor coordinating the review of this manuscript and approving it for publication was Dr. Soontorn Oraintara.

D. E. Quevedo and G. C. Goodwin are with the School of Electrical Engineering & Computer Science, The University of Newcastle, Callaghan, NSW 2308, Australia (e-mail: dquevedo@ieee.org; graham.goodwin@newcastle.edu.au).

H. Bölcskei is with the Communication Technology Laboratory, ETH Zurich, CH-8092, Zurich, Switzerland (e-mail: boelcskei@nari.ee.ethz.ch).

Color versions of one or more of the figures in this paper are available online at http://ieeexplore.ieee.org.

Digital Object Identifier 10.1109/TSP.2008.2008259

a conceptual level, it extends previous work on scalar A/D conversion [15], [16]. (See also related work on discrete coefficient filter design [17] and on channel equalization [18]) to the vector case.

In our approach [which we term a Moving Horizon Subband Quantizer (MHSBQ)], at each time instant, the quantized values are chosen to minimize the energy of a filtered version of the reconstruction error over a (corresponding) finite horizon, together with a "final state weighting" term. The MHSBQ looks ahead at a finite number of "future" samples and effectively performs vector quantization (VQ) over the multiple time instants contained in the horizon. Thus, the MHSBQ amounts to (a special type of) space-time VQ of the K subband signals over multiple time instants.

The main design parameters in the MHSBQ are the horizon length and the final state weighting term. We show that in the special (and simplest) case of the horizon being equal to one and no final state weighting, the MHSBQ reduces to the linear feedback quantizers of [8]. Larger horizons lead to performance improvements. Another advantage of the approach proposed in this paper, when compared to [8], is that stability issues are addressed explicitly. More precisely, we show that, in many situations, the final state weighting term of the MHSBQ can be chosen such that idle tones are suppressed, i.e., we can guarantee that, with a zero input signal, the output signal will decay to zero. Interestingly, these cases are associated with situations where the reconstruction error over a finite horizon together with the final state weighting term essentially amounts to the infinite horizon reconstruction mean-square-error (MSE).

Before proceeding, we note that the subject of scalar $\Sigma\Delta$ quantization of redundant (i.e., oversampled) representations using exact quantization models and explicitly addressing stability issues has recently become a very active area of research in the applied mathematics community; see, e.g., [19]. For representative references the interested reader is referred to [20]–[24]. The approach proposed in the present paper encompasses scalar and subband $\Sigma\Delta$ quantization as a special case and appears to be an entirely new concept in the context of quantization of overcomplete representations. Our stability notion complements those used in [20]–[23]. Whilst in [20]–[23] stability refers to boundedness of signals, our results are concerned with the stronger notion of signals, not only being bounded, but also decaying to zero. In particular, the MHSBQ guarantees absence of idle tones. This is not implied by the results in [20] for scalar $\Sigma\Delta$ quantization. Nevertheless, our results do not resolve the stability problem completely, since they apply only to a specific class of input signals y.

We finally note, that for the scalar $\Sigma\Delta$-based approaches in [20]–[24], it is often possible to compute the reconstruction MSE (or bounds thereon) explicitly as a function of the oversampling factor, see also [25]. Obtaining such explicit results seems to be difficult for the MHSBQ approach presented in this paper and is an important open problem.

The remainder of this paper is organized as follows: In Section II, we review basic concepts related to (oversampled) FBs. Section III presents the proposed MHSBQ. Corresponding design parameters and properties are investigated in Sections IV and V. Section VI documents a simulation study. We conclude in Section VII.

Notation: We adopt vector-space notation to denote signals. For example, in Fig. 1, y denotes the signal $y = \{\ldots, y(-1), y(0), y(1), \ldots\}$. We use upper case bold-face letters for matrices and lower case bold-face letters for vectors and vector-signals; $\mathbf{0}$ denotes the all zeros vector. Unless explicitly specified, the dimension of vectors follows from the context. We use $\mathbf{I}_L$ to denote the $L \times L$ identity matrix and define $\mathbf{0}_K$ to be the all zeros $K \times K$ matrix. Transposition of a matrix is denoted via the superscript ^{T}; the superscript * stands for complex conjugation; the superscript ^{H} denotes conjugate transposition; $\|\mathbf{x}\|_{\mathbf{P}}^2$ stands for the quadratic form $\mathbf{x}^T\mathbf{P}\mathbf{x}$, where $\mathbf{x}$ is any vector and $\mathbf{P}$ is a symmetric positive semidefinite matrix; $\|\mathbf{e}\|^2 \triangleq \mathbf{e}^T\mathbf{e}$. Finally, we will use the following definition of a VQ.

Definition 1 (Euclidean VQ): Consider a finite set of column vectors $\mathcal{B} = \{\mathbf{b}_i\}$, where $\mathbf{b}_i \in \mathbb{R}^{n_\mathcal{B}\times 1}$, $\forall\, \mathbf{b}_i \in \mathcal{B}$, and where $\mathbf{b}_i \neq \mathbf{b}_j, \forall i \neq j$. A nearest neighbor VQ is defined as a mapping $q_\mathcal{B}\colon \mathbb{R}^{n_\mathcal{B}\times 1} \to \mathcal{B}$ which assigns to each vector $\mathbf{c} \in \mathbb{R}^{n_\mathcal{B}\times 1}$ the closest element of $\mathcal{B}$ (as measured by the Euclidean distance), i.e., $q_\mathcal{B}(\mathbf{c}) = \mathbf{b}_i \in \mathcal{B}$ if and only if $\mathbf{c}$ belongs to the region

$$\Big\{\mathbf{c} \in \mathbb{R}^{n_\mathcal{B}\times 1}\colon \|\mathbf{c}-\mathbf{b}_i\|^2 \leq \|\mathbf{c}-\mathbf{b}_j\|^2,\ \forall\, \mathbf{b}_j \neq \mathbf{b}_i,\ \mathbf{b}_j \in \mathcal{B}\Big\}.$$

Note that, in the special case when $n_\mathcal{B} = 1$, the VQ defined above reduces to a scalar quantizer with a scalar output set. In the present paper, we shall, however, be interested in the more general case where $n_\mathcal{B} \geq K$.

II. Background on (Oversampled) Filterbanks

In this section, we give a brief overview of several fundamental aspects of (oversampled) FBs. More thorough treatments can be found, e.g., in [2]–[5], [26], and [27].

A. Basic Aspects

Referring to Fig. 1, the discrete-time input signal y is simultaneously filtered by the analysis filters

$$E_i(z) = \sum_{\ell=-\infty}^{\infty} e_i(\ell) z^{-\ell}, \quad i \in \{1, 2, \ldots, K\}. \tag{1}$$

The K signals y_i are downsampled [1] by a factor of L, i.e., only every Lth sample is retained. The resulting subband sequences v_i are then quantized leading to the K sequences u_i. At each time instant $k \in \mathbb{Z}$, we have

$$u_i(k) \in \mathbb{U}_i, \quad \forall i \in \{1, 2, \ldots, K\} \tag{2}$$

where each of the sets $\mathbb{U}_i$, $i \in \{1, 2, \ldots, K\}$, contains a finite (not necessarily the same) number of elements. The reconstruction error $\hat{y} - y$ clearly depends on how the sequences u_i are chosen inside the abstract quantizer $\mathcal{Q}$. The main focus of this paper is the design of $\mathcal{Q}$ for given sets $\mathbb{U}_i$.[1] A key feature of our approach (which will be presented in Section III) is that we are effectively performing VQ across subchannels and across time. At each time instant $k \in \mathbb{Z}$, the K quantized values $u_i(k)$ in

[1]Of course, joint design of $\mathcal{Q}$ and the $\mathbb{U}_i$ would be interesting, but is beyond the scope of the present paper.

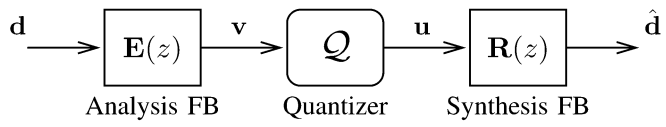

Fig. 2. Oversampled FB in polyphase form.

(2) are jointly designed such as to optimize the quantizer performance. Thus, our strategy is more general than those which simply choose each value $u_i(k)$ separately, i.e., on a subchannel by subchannel basis, via scalar quantizers.

In the synthesis FB, the quantized sequences u_i are upsampled [1] by a factor of L resulting in the sequences w_i. The K filters

$$R_i(z) = \sum_{\ell=-\infty}^{\infty} r_i(\ell) z^{-\ell}, \quad i \in \{1, 2, \ldots, K\} \tag{3}$$

then perform an interpolation/smoothing function, which finally results in the estimate $\hat{y}$.

We define the *oversampling factor* of the FB as

$$r = \frac{K}{L}. \tag{4}$$

B. Polyphase Representation

The oversampled FB of Fig. 1 is a multirate system, which can be represented conveniently in terms of the polyphase description as outlined below; see, e.g., [2], [3], and [27].

We begin by defining the vector sequences

$$\mathbf{v}(k) \triangleq \begin{bmatrix} v_1(k) \\ v_2(k) \\ \vdots \\ \vdots \\ v_K(k) \end{bmatrix} \quad \mathbf{u}(k) \triangleq \begin{bmatrix} u_1(k) \\ u_2(k) \\ \vdots \\ \vdots \\ u_K(k) \end{bmatrix}$$
$$\mathbf{d}(k) \triangleq \begin{bmatrix} d_1(k) \\ d_2(k) \\ \vdots \\ d_L(k) \end{bmatrix} \quad \hat{\mathbf{d}}(k) \triangleq \begin{bmatrix} \hat{d}_1(k) \\ \hat{d}_2(k) \\ \vdots \\ \hat{d}_L(k) \end{bmatrix} \tag{5}$$

where

$$d_i(k) \triangleq y(kL + i - 1), \quad i \in \{1, 2, \ldots, L\}$$
$$\hat{d}_i(k) \triangleq \hat{y}(kL + i - 1), \quad i \in \{1, 2, \ldots, L\} \tag{6}$$

are the polyphase components of y and $\hat{y}$, respectively. Note that the vectors defined in (5) are updated only every L sampling instants of y.

By using the so-called *noble identities*, see, e.g., [3], direct algebraic manipulation yields that the FB of Fig. 1 can be characterized via:[2]

$$\mathbf{v} = \mathbf{E}(z)\mathbf{d}$$
$$\hat{\mathbf{d}} = \mathbf{R}(z)\mathbf{u}. \tag{7}$$

[2]Here, and in some expressions to follow, z should be interpreted as the forward shift operator. For example, $\mathbf{v}$ in (7) is the output sequence of the LTI system $\mathbf{E}(z)$ with input sequence $\mathbf{d}$.

Here, $\mathbf{E}(z)$ is the $K \times L$ *analysis polyphase matrix*, while $\mathbf{R}(z)$ is the $L \times K$ *synthesis polyphase matrix*, defined as

$$[\mathbf{E}(z)]_{i,n} = E_{i,n}(z), \quad i \in \{1, 2, \ldots, K\}, \quad n \in \{1, 2, \ldots, L\}$$

and

$$[\mathbf{R}(z)]_{n,i} = R_{i,n}(z), \quad i \in \{1, 2, \ldots, K\}, \quad n \in \{1, 2, \ldots, L\}$$

respectively, with the polyphase filters

$$E_{i,n}(z) \triangleq \sum_{\ell=-\infty}^{\infty} e_i(\ell L - n + 1) z^{-\ell}$$
$$R_{i,n}(z) \triangleq \sum_{\ell=-\infty}^{\infty} r_i(\ell L + n - 1) z^{-\ell}.$$

The resulting equivalent scheme is depicted in Fig. 2 showing the polyphase description of a multi-input multi-output (MIMO) single-rate system, which operates on the downsampled signals.

C. Perfect Reconstruction

In the absence of quantization, perfect reconstruction, i.e., $\hat{y} = y$, is obtained by ensuring

$$\mathbf{R}(z)\mathbf{E}(z) = \mathbf{I}_L. \tag{8}$$

FBs which satisfy (8) are termed *perfect reconstruction* FBs [3]. Note that choosing $\mathbf{R}(z)$ as any left-inverse of $\mathbf{E}(z)$ will result in a perfect reconstruction FB [27]. (Note that the left-inverse of $\mathbf{E}(z)$ is nonunique only in the oversampled case, where $r > 1$. When $r = 1$, (8) requires $\mathbf{R}(z) = \mathbf{E}(z)^{-1}$; in which case $\mathbf{E}(z)$ needs to be invertible.) In particular, if quantization effects are modeled as additive white Gaussian noise, then choosing $\mathbf{R}(z)$ as the para-pseudoinverse of $\mathbf{E}(z)$, i.e., $\mathbf{R}(z) = (\tilde{\mathbf{E}}(z)\mathbf{E}(z))^{-1}\tilde{\mathbf{E}}(z)$,[3] will minimize the reconstruction MSE [8]. Other approaches to the design of $\mathbf{R}(z)$ taking into account quantization effects can be found, for example, in [9], [10], and [28].

D. Quantization Aspects

Quantization commonly induces a loss of information when transforming the sequence $\mathbf{v}$ into the sequence $\mathbf{u}$. As a consequence, the reconstructed sequence $\hat{\mathbf{d}}$ will differ from $\mathbf{d}$, in general, i.e., the *reconstruction error*, which we define as

$$\mathbf{e}_d \triangleq \mathbf{d} - \hat{\mathbf{d}} \tag{9}$$

will be nonzero. Note that, given (5) and (6), the sequence $\mathbf{e}_d$ can alternatively be characterized via

$$\mathbf{e}_d(k) = \begin{bmatrix} y(kL) \\ y(kL+1) \\ \vdots \\ y(kL+L-1) \end{bmatrix} - \begin{bmatrix} \hat{y}(kL) \\ \hat{y}(kL+1) \\ \vdots \\ \hat{y}(kL+L-1) \end{bmatrix}, \quad k \in \mathbb{Z}. \tag{10}$$

[3]Here, $\tilde{\mathbf{E}}(z) = \mathbf{E}^H(1/z^*)$ is the para-conjugate of $\mathbf{E}(z)$.

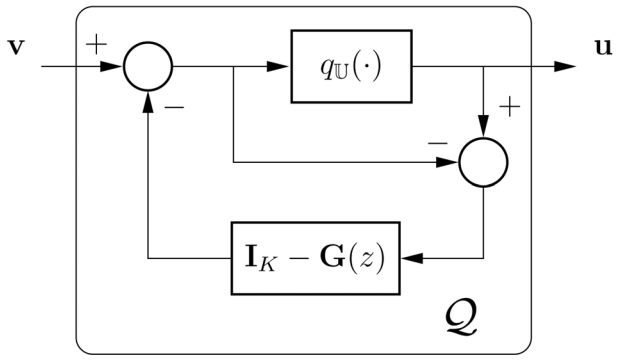

Fig. 3. Noise-shaping quantizer.

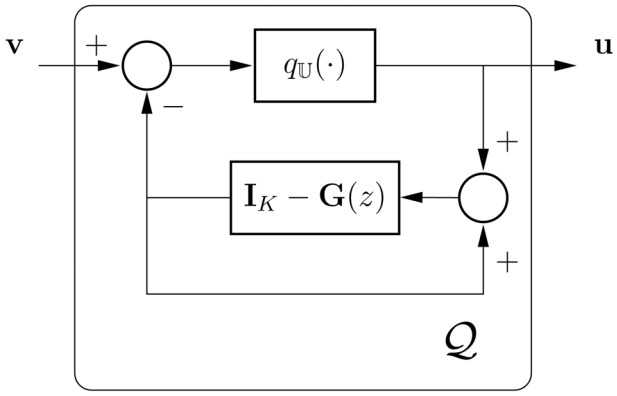

Fig. 4. Signal predictive quantizer.

As stated in [3], the effect of quantization of the subband sequences is very difficult to analyze exactly. The usual paradigm adopted models the quantizer by a linear gain-plus-noise model, as in the case of standard A/D conversion; see, e.g., [29]. This model is simple and may, in some cases, yield useful results, see also [30]. Nevertheless, it fails to predict nonlinear effects, such as the appearance of idle tones or chaotic output sequences; see, e.g., [31].

A simple subband quantization method is described in [3] and [32]. It uses one scalar quantizer for each subband, i.e., it sets

$$u_i(k) = q_{\mathbb{U}_i}(v_i(k)), \qquad \forall k \in \mathbb{Z}, \quad \forall i \in \{1, 2, \ldots, K\} \tag{11}$$

where we have used the notation introduced in Definition 1, with $n_{\mathcal{B}} = 1$ and $\mathcal{B} = \mathbb{U}_i$. Based upon the linear quantization paradigm aforementioned, the number of bits assigned to each quantizer can be determined according to the energy content of each subband sequence in an optimal manner. This type of methodology is widespread, especially in audio coding applications; see, e.g., [6] and [33].

E. Linear Feedback Subband Quantization

Oversampled FBs provide redundant expansions of the input signal y, see [26] and [27]. In [8] it was shown how this redundancy can be exploited to reduce quantization errors in $\hat{y}$ through the use of linear feedback quantization methods, i.e., the noise-shaping quantizer depicted in Fig. 3 and the signal predictive quantizer in Fig. 4. As can be seen in those figures, linear feedback quantizers incorporate feedback loops which contain a linear MIMO filter $\mathbf{G}(z)$ of dimension $K \times K$. These quantizers essentially correspond to MIMO versions of $\Sigma\Delta$-converters and noise-shaping quantizers; see, e.g., [12] and [13].[4]

The architecture in [8] (see Figs. 3 and 4) amounts to subchannel by subchannel quantization, i.e.

$$\mathbf{u}(k) \in \mathbb{U}, \quad \forall k \in \mathbb{Z} \tag{12}$$

where the set $\mathbb{U}$ is defined via

$$\mathbb{U} \triangleq \mathbb{U}_1 \times \mathbb{U}_2 \times \cdots \times \mathbb{U}_K \subset \mathbb{R}^K \tag{13}$$

[4]Compare also to parallel $\Sigma\Delta$-Converter structures as described, for example, in [34].

see (2). Based on the linear quantization model one can then design an *optimal*, in the sense of minimizing the reconstruction MSE, filter $\mathbf{G}(z)$, see [8], [11].

In the next section, we propose a novel quantization method for oversampled FBs. As will be apparent, the new scheme embeds linear feedback quantization in a broader framework and contains noise shaping and signal predictive subband quantizers as special cases. The method does not rely on an additive white quantization noise model and allows one to enforce stability of the feedback loop.

III. Moving Horizon Subband Quantization

The main aim of the abstract quantizer $\mathcal{Q}$ in Fig. 1 is to make the reconstruction error $\mathbf{e}_d$ [defined in (9)] small by appropriate selection of $\mathbf{u}$, for fixed and given $\mathbb{U}$. In what follows, we will use methods stemming from the Model Predictive Control framework, see, e.g., [35] and [36], to design a subband quantizer, which minimizes a weighted measure of the reconstruction error. On a conceptual level, the proposed method extends our previous work on (scalar) signal quantization documented in [15] and [16] to oversampled FBs or, equivalently, to nonsquare MIMO systems. The quantization scheme to be presented will be seen to also outperform the linear feedback subband quantizers of [8].

A. Frequency-Selective Subband Quantization

The subband quantization problem outlined above can be embedded into the more general problem of minimizing the filtered distortion sequence

$$\mathbf{e}_f \triangleq \mathbf{W}(z)(\mathbf{H}(z)\mathbf{d} - \mathbf{u}) \tag{14}$$

subject to the vector sequence $\mathbf{u}$, see (5), taking values in the set $\mathbb{U}$ defined in (13). In (14), $\mathbf{H}(z)$ is of dimension $K \times L$ and $\mathbf{W}(z)$ is a causal filter of dimension $n_e \times K$, where $n_e \in \mathbb{N}$.

As an example of this setting, consider a perfect reconstruction FB, see (8), and choose $\mathbf{H}(z) = \mathbf{E}(z)$ and $\mathbf{W}(z) = \mathbf{R}(z)$. In this case, $\mathbf{e}_f$ corresponds to the reconstruction error $\mathbf{e}_d$ defined in (9).

More generally, the two filters $\mathbf{H}(z)$ and $\mathbf{W}(z)$ allow the designer to consider a (frequency-) weighted reconstruction error.

Indeed, if $\mathbf{e}_f$ is minimized (in some appropriate sense), then $\mathbf{u}$ will approximate the sequence

$$\mathbf{a} \triangleq \mathbf{H}(z)\mathbf{d} \tag{15}$$

and $\mathbf{W}(z)$ in (14) weights the signal $\mathbf{a}-\mathbf{u}$ in a frequency-selective manner. More details on how to choose $\mathbf{W}(z)$ and $\mathbf{H}(z)$ are provided later in Section IV-B. For now, we focus on the problem of minimizing $\mathbf{e}_f$ for fixed filters $\mathbf{W}(z)$ and $\mathbf{H}(z)$.

For the ensuing discussion, it is convenient to use a state-space description and to characterize $\mathbf{W}(z)$ via

$$\mathbf{W}(z) = \mathbf{D} + \mathbf{C}(z\mathbf{I}_n - \mathbf{A})^{-1}\mathbf{B} \tag{16}$$

where $n \in \mathbb{N}$ is the order of the chosen filter $\mathbf{W}(z)$, $\mathbf{A} \in \mathbb{R}^{n\times n}$, $\mathbf{B} \in \mathbb{R}^{n\times K}$, $\mathbf{C} \in \mathbb{R}^{n_e\times n}$, and where $\mathbf{D} \in \mathbb{R}^{n_e\times K}$ is nonzero. Based on (16), we have

$$\begin{aligned}\mathbf{e}_f(k) &= \mathbf{C}\mathbf{x}(k) + \mathbf{D}(\mathbf{a}(k) - \mathbf{u}(k))\\ \mathbf{x}(k+1) &= \mathbf{A}\mathbf{x}(k) + \mathbf{B}(\mathbf{a}(k) - \mathbf{u}(k))\end{aligned} \tag{17}$$

where $\mathbf{x}$ is the filter state.[5]

B. Optimization Criterion

Given the setting described above, the subband quantizer can now be designed with an optimality criterion in mind. More precisely, we will focus on the energy of the filtered distortion sequence $\mathbf{e}_f$. For that purpose, at every time instant k, we propose to minimize the following measure of $\mathbf{e}_f$ defined over a finite and fixed horizon $N \in \mathbb{N}$

$$V_N(\vec{\mathbf{u}}(k); \mathbf{x}(k)) \triangleq \|\mathbf{x}'(k+N)\|^2_{\mathbf{P}} + \sum_{\ell=k}^{k+N-1} \|\mathbf{e}'_f(\ell)\|^2 \tag{18}$$

where $\mathbf{P} \in \mathbb{R}^{n\times n}$ is a given positive semidefinite matrix and

$$\vec{\mathbf{u}}(k) \triangleq \begin{bmatrix} \mathbf{u}'(k) \\ \mathbf{u}'(k+1) \\ \vdots \\ \mathbf{u}'(k+N-1) \end{bmatrix} \in \mathbb{U}^N \subset \mathbb{R}^{NK\times 1} \tag{19}$$

contains the decision variables (quantized values). The constraint set $\mathbb{U}$ underlying the cost function (18) is defined in (13); primed variables refer to "potential values" of the filtered distortion $\mathbf{e}_f$ and the *final* state $\mathbf{x}(k+N)$, which would result if the quantizer outputs $\{\mathbf{u}(k), \mathbf{u}(k+1), \ldots, \mathbf{u}(k+N-1)\}$ were set equal to the corresponding values in $\vec{\mathbf{u}}(k)$. In accordance with (17), these potential trajectories are formed as

$$\begin{aligned}\mathbf{e}'_f(\ell) &= \mathbf{C}\mathbf{x}'(\ell) + \mathbf{D}(\mathbf{a}(\ell) - \mathbf{u}'(\ell))\\ \mathbf{x}'(\ell+1) &= \mathbf{A}\mathbf{x}'(\ell) + \mathbf{B}(\mathbf{a}(\ell) - \mathbf{u}'(\ell))\end{aligned} \tag{20}$$

with $\ell \in \{k, k+1, \ldots, k+N-1\}$.

The initial condition in (20) is

$$\mathbf{x}'(k) = \mathbf{x}(k)$$

which is uniquely determined from past values of $\mathbf{u}$ and of $\mathbf{d}$. To be more precise, due to (15), the sequence $\{\mathbf{d}(0), \mathbf{d}(1), \ldots, \mathbf{d}(k-1)\}$ gives rise to the sequence $\{\mathbf{a}(0), \mathbf{a}(1), \ldots, \mathbf{a}(k-1)\}$. The vector sequence $\mathbf{x}$ can then be calculated via the recursion, see (17)

$$\mathbf{x}(k) = \mathbf{A}\mathbf{x}(k-1) + \mathbf{B}(\mathbf{a}(k-1) - \mathbf{u}(k-1)) \tag{21}$$

initialized with $\mathbf{x}(0) = \mathbf{0}$.

Minimization of V_N in (18) at time instant k gives rise to the optimizer

$$\vec{\mathbf{u}}^\star(k) \triangleq \arg \min_{\vec{\mathbf{u}}(k)\in\mathbb{U}^N} V_N(\vec{\mathbf{u}}(k); \mathbf{x}(k)). \tag{22}$$

Clearly, (22) amounts to (a special type of) space-time VQ of the K subband signals over the multiple time instants contained in the horizon window. Indeed, the solution $\vec{\mathbf{u}}^\star(k)$ of the optimization problem contains values which, in principle, could be used in the sequence $\mathbf{u}$ (see Fig. 2) at instants $k, k+1, \ldots, k+N-1$, see (19). To obtain better performance, in Section III-C, we will present an alternative strategy, where minimizations are carried out at every time instant, thus, providing a sequence of optimizers $\{\vec{\mathbf{u}}^\star(0), \vec{\mathbf{u}}^\star(1), \ldots\}$. The sequence $\mathbf{u}$ is then obtained by setting each $\mathbf{u}(k)$, $k \in \mathbb{N}$ equal to the first element of $\vec{\mathbf{u}}^\star(k)$ [which is of dimension $K\times 1$ and contains values for all K subchannels for instant k, see (19)].

Remark 1 (Decision Delay): An important feature of (22) is that $\vec{\mathbf{u}}^\star(k)$ is obtained through "looking ahead" at the signal $\mathbf{d}$ up until time instant $k+N-1$. Thus, the quantizer incurs a decision delay of N time steps (or, equivalently, NL samples of y) plus the time required to compute the optimizer in (22). △

Before proceeding, we emphasize that a key aspect of our approach is the inclusion of the final state weighting term $\|\mathbf{x}'(k+N)\|^2_{\mathbf{P}}$ in V_N. As is known from the systems and control literature, see, for example, [36], final state weighting can, at times, be used as a mechanism to approximate *infinite horizon* behavior via a *finite-horizon* cost function. In fact, the following result shows that (in the case of stable filters $\mathbf{W}(z)$), through proper choice of the matrix $\mathbf{P}$, we can, indeed, approximate the minimization of the energy of $\mathbf{e}_f$ over an infinite horizon through the use of the finite-horizon cost function (18).

Lemma 1 (Infinite Horizons): Suppose that $\mathbf{W}(z)$ is a stable filter, i.e., all eigenvalues of $\mathbf{A}$ in (16) lie strictly inside the unit circle, and that $\mathbf{u}'(\ell)$ is equal to $\mathbf{a}(\ell)$ for every $\ell \geq k+N$. If the matrix $\mathbf{P}$ in (18) satisfies the Lyapunov Equation

$$\mathbf{A}^T\mathbf{P}\mathbf{A} + \mathbf{C}^T\mathbf{C} = \mathbf{P} \tag{23}$$

we have

$$V_N(\vec{\mathbf{u}}(k); \mathbf{x}(k)) = \sum_{\ell=k}^{\infty} \|\mathbf{e}'_f(\ell)\|^2. \tag{24}$$

Proof: The proof uses basic properties of linear systems, as described, for example, in [38]. We first note that, since (16) is a minimal realization of the stable system $\mathbf{W}(z)$, we have that $\mathbf{C}^T\mathbf{C}$ is positive definite and the Lyapunov Equation (23) has a unique solution; see, e.g., [37].

On the other hand, it follows directly from (20) that, if $\mathbf{u}'(\ell) = \mathbf{a}(\ell)$, $\forall \ell \geq k+N$, then: (see the equation at the bottom of the next page). Direct substitution confirms that $\mathbf{P} = \sum_{i=0}^{\infty} (\mathbf{A}^T)^i \mathbf{C}^T\mathbf{C}\mathbf{A}^i$, indeed, satisfies (23). Thus,

[5]The state-space description adopted encompasses all causal rational- and FIR-filters with a nonzero direct feedthrough term. If $\mathbf{W}(z)$ is chosen to be a rational filter, then n corresponds to its number of poles, i.e., to the number of roots of the denominator polynomials in the Smith-McMillan form of $\mathbf{W}(z)$. If $\mathbf{W}(z)$ is chosen to be an FIR-filter, then $n+1$ is the impulse response length; see, e.g., [37].

$\|\mathbf{x}'(k+N)\|_{\mathbf{P}}^2 = \sum_{\ell=k+N}^{\infty} \|\mathbf{e}_f'(\ell)\|^2$. The result (24) now follows from (18). ■

We note that the quantized nature of $\mathbf{u}'$ will generally preclude $\mathbf{u}'(\ell)$ from being equal to $\mathbf{a}(\ell)$ for every $\ell \geq k+N$ and (24) is, therefore, only approximate. Nevertheless, as will become clear in Section IV-C, choosing $\mathbf{P}$ as the unique solution of the Lyapunov Equation (23) helps to ensure idle tone suppression.

C. Moving Horizon Optimization

The basic idea of this paper is to use the moving horizon principle as described, for example, in [36]. In this paradigm, at every time instant k the finite horizon cost function V_N in (18) is minimized over a corresponding horizon. The output of the abstract quantizer is set to

$$\mathbf{u}(k) \longleftarrow \mathbf{u}^{\star}(k) \tag{25}$$

where the vector

$$\mathbf{u}^{\star}(k) \triangleq [\,\mathbf{I}_K \quad \mathbf{0}_K \quad \ldots \quad \mathbf{0}_K\,]\,\vec{\mathbf{u}}^{\star}(k) \tag{26}$$

is obtained from the solution of (22).

In our approach, $\mathbf{u}^{\star}(k)$ is then used in (17) to deliver the successor state $\mathbf{x}(k+1)$ according to

$$\mathbf{x}(k+1) = \mathbf{A}\mathbf{x}(k) + \mathbf{B}(\mathbf{a}(k) - \mathbf{u}^{\star}(k)). \tag{27}$$

In the next time instant, $\mathbf{x}(k+1)$ is used to minimize the cost function $V_N(\vec{\mathbf{u}}(k+1); \mathbf{x}(k+1))$, yielding $\mathbf{u}(k+1) = \mathbf{u}^{\star}(k+1)$, see (26). This procedure is repeated *ad-infinitum*. As illustrated in Fig. 5, for a horizon of $N = 5$, the *time window* used in the minimization of V_N slides forward as k increases. The past is propagated forward in time via the state sequence $\mathbf{x}$.[6]

Fig. 6 schematizes the proposed subband quantizer. We will term it a MHSBQ. Clearly, the MHSBQ is a time-varying subband quantization scheme.

Remark 2 (Relationship to Model Predictive Control): The MHSBQ can be regarded as a particular MIMO Model Predictive Controller, see, e.g., [35] and [36], with *plant* $\mathbf{W}(z)$, *controlled input* $\mathbf{u}$ and *reference signal* $\mathbf{W}(z)\mathbf{H}(z)\mathbf{d}$. A special feature of the particular situation at hand is that $\mathbf{u}$ is restricted to satisfy the quantization constraint (12). This puts the subband quantization problem into the finite set constrained predictive control framework developed recently in [14]. △

[6]Note that due to the Markov-property (17), the effect of $\{\mathbf{u}(\ell), \mathbf{a}(\ell)\}_{\ell<k}$ on $\{\mathbf{e}_f(k+j)\}_{j\geq 0}$ is summarized by the state $\mathbf{x}(k)$.

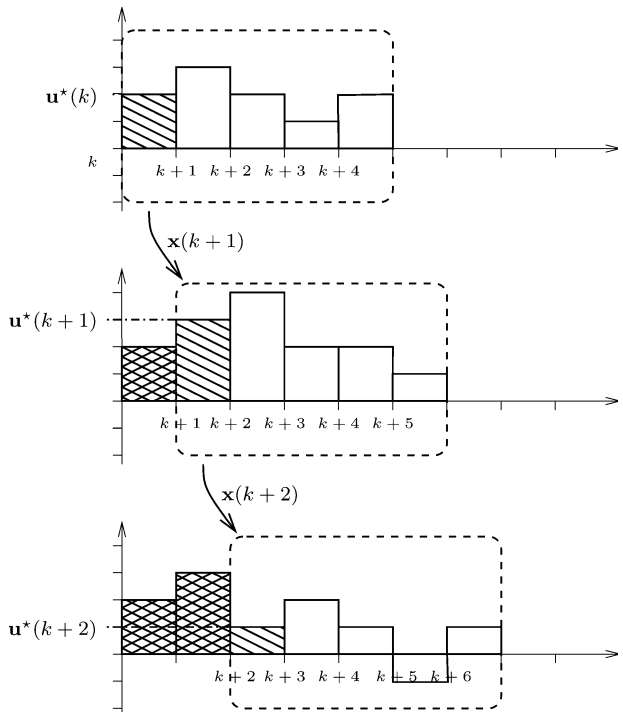

Fig. 5. Moving horizon optimization $N = 5$.

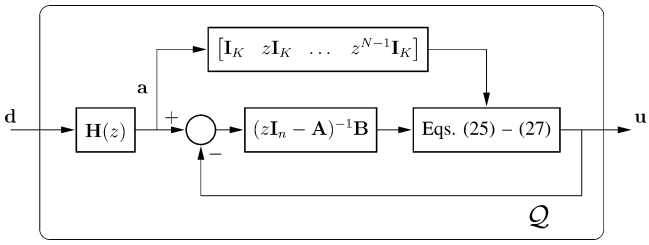

Fig. 6. The MHSBQ.

IV. Design Parameters

In this section, we will provide some details on the role of the MHSBQ design parameters N, $\mathbf{H}(z)$, $\mathbf{W}(z)$ and $\mathbf{P}$.

A. Optimization Horizon N

Given (18), it is easy to see that, in general, larger values for the optimization horizon N provide better performance since more information about the associated filtered distortion is taken into account when choosing the quantized subband sequences. In addition, one can expect that, for large enough N, the effect of $\mathbf{u}(k)$ on $\mathbf{e}_f(\ell)$ for $\ell \geq k+N$ will be negligible and, consequently, the MHSBQ will give the same performance as if an infinite horizon were used. (Note that, as shown in Section III-B, the final state weighting term can be used to emulate infinite horizon behavior for finite N.)

$$\sum_{\ell=k+N}^{\infty} \|\mathbf{e}_f'(\ell)\|^2 = \sum_{\ell=k+N}^{\infty} \|\mathbf{C}\mathbf{x}'(\ell)\|^2$$
$$= (\mathbf{x}'(k+N))^T \left(\sum_{i=0}^{\infty} (\mathbf{A}^T)^i \mathbf{C}^T \mathbf{C} \mathbf{A}^i \right) \mathbf{x}'(k+N).$$

On the other hand, as already mentioned in Remark 1, choosing large horizons incurs large decision delays. Solving the combinatorial program needed to obtain $\vec{\mathbf{u}}^{\star}(k)$ in (22) for recursive filters $\mathbf{W}(z)$, results in exponential complexity in N.[7],[8] If $\mathbf{W}(z)$ is FIR, then the optimization can be carried out following a Viterbi Algorithm-like approach [41], and has computational complexity which is only linear in N, see also [18].

As a consequence, the optimization horizon parameter N allows the designer to trade-off performance for on-line computational effort. Fortunately, as will be demonstrated in simulation studies (see Sections V-B and VI), excellent performance can often be achieved with relatively small horizons.

B. Weighting Filters $\mathbf{W}(z)$ and $\mathbf{H}(z)$

As already outlined in Section III-A, the frequency weighting filter $\mathbf{W}(z)$ and the prefilter $\mathbf{H}(z)$ in (14) can be utilized to (implicitly) specify spectral characteristics of the subband sequences u_i and of the resultant reconstruction error $\mathbf{e}_d$.

One possible design choice motivated by the specific problem considered in this paper is as follows:

$$\mathbf{H}(z) = \mathbf{E}(z), \quad \mathbf{W}(z) = z^{-\delta}\mathbf{R}(z) \tag{28}$$

where δ is the unique integer such that $z^{-\delta}\mathbf{R}(z)$ is causal with nonzero direct feedthrough. In this case, the input to the quantizer in Fig. 6 is given by $\mathbf{a} = \mathbf{v}$. Moreover, (7) and (14) yield

$$\mathbf{e}_f = z^{-\delta}\mathbf{R}(z)(\mathbf{E}(z)\mathbf{d} - \mathbf{u}) = z^{-\delta}\left(\mathbf{R}(z)\mathbf{E}(z)\mathbf{d} - \hat{\mathbf{d}}\right) \tag{29}$$

i.e., $\mathbf{e}_f$ corresponds to the difference between (possibly delayed versions of) the reconstructed sequence $\hat{\mathbf{d}}$ and the reconstructed sequence which would be obtained in the absence of quantization effects.

Furthermore, if $\mathbf{E}(z)$ and $\mathbf{R}(z)$ are chosen to correspond to a perfect reconstruction FB, see (8), then (29) yields

$$\mathbf{e}_f = z^{-\delta}(\mathbf{d} - \hat{\mathbf{d}}) = z^{-\delta}\mathbf{e}_d. \tag{30}$$

Consequently, with (28) and $\mathbf{R}(z)\mathbf{E}(z) = \mathbf{I}_L$, the MHSBQ minimizes the energy of $\mathbf{e}_d$ via a moving horizon approach. As already mentioned in Sections III-B and IV-A, the moving horizon strategy serves as a practical approximation to infinite-horizon optimal designs. Lemma 1 gives an indication of the quality of the approximation.[9]

Certainly, other design choices for $\mathbf{W}(z)$ and $\mathbf{H}(z)$ are possible. For example, one can incorporate psycho-acoustical aspects into the subband quantizer, by choosing $\mathbf{W}(z)$ accordingly. Also, in Section V, we will outline an alternative design procedure for $\mathbf{W}(z)$ and $\mathbf{H}(z)$, which will relate the proposed approach to linear feedback quantization principles and show that $\Sigma\Delta$ and signal predictive subband quantizers are special cases of the MHSBQ.

C. Final State Weighting Matrix $\mathbf{P}$

A very significant, but largely unsolved, issue which arises when including a quantizer in a feedback loop is that of stability. Poor stability properties manifest themselves in the appearance of nonlinear phenomena such as limit cycles (in particular, idle tones) and chaotic trajectories, see also [14], [31], [42], and [43]. In particular, even with zero input, architectures such as (undithered) scalar and subband $\Sigma\Delta$-converters and also the MHSBQ introduced in Section III, may produce nonzero outputs (idle tones) that do not decay over time. In general, it cannot be guaranteed that quantization-induced errors will decay.

We will next show how the final state weighting term in the cost function (18) can be used to suppress idle tones in the MHSBQ for any horizon N, prefilter $\mathbf{H}(z)$ and stable weighting filter $\mathbf{W}(z)$. The following result generalizes [16, Theorem 2] to the MIMO case.

Theorem 1: Suppose that the sequence $\mathbf{a}$ is such that, for a finite value $k \in \mathbb{N}$, we have

$$\mathbf{a}(\ell) \in \mathbb{U}, \quad \forall \ell \geq k. \tag{31}$$

Then, if $\mathbf{P}$ is chosen to satisfy the Lyapunov Equation (23), we have

$$\lim_{\ell \to \infty} \mathbf{e}_f(\ell) = \mathbf{0}.$$

Proof: The proof is included in the Appendix. ■

While Theorem 1 is applicable to a very restricted class of input signals, it does guarantee that idle tones will not occur, provided $0 \in \mathbb{U}_i$, $\forall i \in \{1, 2, \ldots, K\}$. It should be emphasized that, case studies, such as those included in Section VI, indicate that setting $\mathbf{P}$ equal to the *stabilizing* choice given in (23) tends to avoid limit cycles even for more general input signals.

Remark 3 (Relationship to Other Stability Results): If $K = L = 1$, then the MHSBQ scheme is conceptually equivalent to the multistep optimal A/D converter presented in [16]. If, in this scalar case, the optimization horizon is chosen as $N = 1$, then it was shown in [16] that $\Sigma\Delta$-converter architectures are obtained. Thus, $\Sigma\Delta$-converters are contained within our framework as a very particular and simple special case. Consequently, it is worth putting our result into perspective with respect to existing results on the stability of $\Sigma\Delta$-converters.[10]

Theorem 1 concerns all MHSBQs, such that $\mathbf{W}(z)$ is stable, $\mathbf{P}$ solves (23) and the input signal and $\mathbf{H}(z)$ are such that (31) is satisfied, in which case we have $\lim_{\ell \to \infty} \mathbf{x}(\ell) = \mathbf{0}$. (Note that, in this case, it directly follows that the state sequence $\mathbf{x}$ is bounded, since the MHSBQ corresponds to a stable system driven by bounded input signals, see Fig. 6.) Thus, the result does not apply to designs where $\mathbf{W}(z)$ has integrators in one (or

[7]Computation times to solve (22) are, in general, also exponential in the number of subband sequences K.

[8]Note that by adapting recent developments in the general VQ framework, see, e.g., [39], [40], optimization algorithms may be conceived, which have an average-case complexity which is lower than explicit exhaustive search.

[9]It is worth mentioning here that in [8] a linear quantization model is used to find feedback filters in linear feedback subband quantizers such that the variance of $\mathbf{e}_d$ is minimized. In contrast to [8], the design choice (28) is immediate and does not rest upon a linear quantization model. Furthermore, in Section V we will show that the MHSBQ generalizes and, in general, outperforms the linear feedback quantizers in [8].

[10]In Section V-B, we show that for $N = 1$ the MHSBQ is equivalent to the linear feedback subband quantization architectures presented in [8].

more) of the scalar subchannels.[11] It should also be noted that the condition (31) is rather restrictive and seems to be useful only for idle tone suppression

Most existing analytical stability results available in the scalar $\Sigma\Delta$-converter literature, see, e.g., [20]–[23], only concern specific designs of the feedback filter, typically those with integrators. The stability notion employed in [20]–[23] amounts to boundedness of state and converter output trajectories for bounded inputs. This is useful for establishing the behavior of the reconstruction MSE as a function of oversampling ratio, but does not address the issue of idle tones. In summary, Theorem 1, complements existing results. The class of systems considered is broader and the stability notion is different. $\triangle$

V. Relationship to Linear Feedback Subband Quantizers

As stated in Section III-A, the frequency weighting filter $\mathbf{W}(z)$ is of dimension $n_e \times K$. In Section IV-B we proposed to choose $\mathbf{W}(z)$ via (28), in which case $n_e = L$. In the present section, we will focus on designs where $n_e = K$ and show that MHSBQs generalize the linear feedback subband quantizers in [8].

A. Closed Form Solution

The subband quantizer proposed in Section III requires that one solve the nonconvex finite-set-constrained optimization problem (22) at every time step (of $\mathbf{d}$). In the particular case of a square filter $\mathbf{W}(z)$ of dimension $K \times K$, i.e., of choosing $n_e = K$, see Section III-A, we can extend the results in [16], to the vector-valued case, in order to interpret the MHSBQ in terms of a VQ immersed in a feedback loop. For that purpose, it is convenient to define the matrices[12]

$$\mathbf{\Gamma} \triangleq \begin{bmatrix} \mathbf{C} \\ \mathbf{CA} \\ \vdots \\ \mathbf{CA}^{N-1} \end{bmatrix}, \ \mathbf{\Phi} \triangleq \begin{bmatrix} \mathbf{W}_0 & \mathbf{0} & \dots & \mathbf{0} \\ \mathbf{W}_1 & \mathbf{W}_0 & \ddots & \vdots \\ \vdots & \ddots & \ddots & \mathbf{0} \\ \mathbf{W}_{N-1} & \dots & \mathbf{W}_1 & \mathbf{W}_0 \end{bmatrix}$$
$$\mathbf{M} \triangleq [\,\mathbf{A}^{N-1}\mathbf{B} \quad \mathbf{A}^{N-2}\mathbf{B} \quad \dots \quad \mathbf{AB} \quad \mathbf{B}\,]. \tag{32}$$

In the above definition

$$\mathbf{W}_0 \triangleq \mathbf{D}, \quad \mathbf{W}_i \triangleq \mathbf{CA}^{i-1}\mathbf{B}, \quad i \in \{1, 2, \dots, N-1\},$$

see (16). Thus, the columns of $\mathbf{\Phi}$ are truncated versions of the impulse response corresponding to $\mathbf{W}(z)$.

Furthermore, we introduce the $NK \times K$ filters

$$\mathbf{\Upsilon}(z) \triangleq \mathbf{\Psi}^{-T}\left(\mathbf{\Phi}^T\mathbf{\Gamma} + \mathbf{M}^T\mathbf{P}\mathbf{A}^N\right)(z\mathbf{I}_n - \mathbf{A})^{-1}\mathbf{B},$$
$$\mathbf{\Omega}(z) \triangleq \mathbf{\Psi}\,[\,\mathbf{I}_K \quad z\mathbf{I}_K \quad \dots \quad z^{N-1}\mathbf{I}_K\,]^T + \mathbf{\Upsilon}(z) \tag{33}$$

[11]Whilst stability cannot be ensured in these cases, simulation studies have shown that (in the related context of scalar A/D conversion) the moving horizon optimization approach gives significant performance gains when compared to standard $\Sigma\Delta$-conversion approaches [16].

[12]For further details, the interested reader is referred to [16].

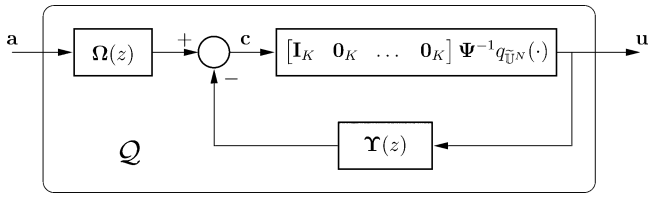

Fig. 7. Implementation of the MHSBQ as a feedback loop, $n_e = K$.

where the matrix $\mathbf{\Psi} \in \mathbb{R}^{NK \times NK}$ is obtained from the factorization

$$\mathbf{\Psi}^T\mathbf{\Psi} = \mathbf{\Phi}^T\mathbf{\Phi} + \mathbf{M}^T\mathbf{P}\mathbf{M}. \tag{34}$$

With this, we obtain the following result.

Lemma 2: Suppose that $\mathbb{U}^N = \{\mathbf{s}_1, \mathbf{s}_2, \dots, \mathbf{s}_r\}$, where[13] $r = |\mathbb{U}|^N$ and that $\mathbf{W}(z)$ has realization (16), with $\mathbf{D} \in \mathbb{R}^{K \times K}$, then the output of the MHSBQ at any time instant k is given by

$$\mathbf{u}(k) = [\,\mathbf{I}_K \quad \mathbf{0}_K \quad \dots \quad \mathbf{0}_K\,]\,\mathbf{\Psi}^{-1}q_{\widetilde{\mathbb{U}}^N}(\mathbf{c}(k)) \tag{35}$$

where the signal $\mathbf{c}$ satisfies

$$\mathbf{c} \triangleq \mathbf{\Omega}(z)\mathbf{H}(z)\mathbf{d} - \mathbf{\Upsilon}(z)\mathbf{u} \tag{36}$$

and $q_{\widetilde{\mathbb{U}}^N}(\cdot)$ is a Euclidean VQ (see Definition 1) with image being given by the set

$$\widetilde{\mathbb{U}}^N \triangleq \{\tilde{\mathbf{s}}_1, \tilde{\mathbf{s}}_2, \dots, \tilde{\mathbf{s}}_r\} \tag{37}$$

which is obtained, term-wise, from $\mathbb{U}^N$ via

$$\tilde{\mathbf{s}}_j = \mathbf{\Psi}\mathbf{s}_j, \quad \mathbf{s}_j \in \mathbb{U}^N, \quad j \in \{1, 2, \dots, r\}.$$

Proof: The proof of Lemma 2 follows closely that of Theorem 1 in [16] and is omitted here for the sake of brevity. ■

The above result leads directly to the closed loop implementation of the MHSBQ depicted in Fig. 7. It should be emphasized that, if $\mathbf{W}(z)$ is not square, then Fig. 7 does not apply.

B. Relationship to Linear Feedback Quantization

The developments in the previous section set the stage for showing that subband linear feedback quantization methods, as introduced in [8], are contained in the class of MHSBQs studied in this paper.

To establish this relationship more formally, consider the special (and simple) case of horizon $N = 1$, and a square frequency weighting filter $\mathbf{W}(z)$ with $n_e = K$ and where $\mathbf{D} = \mathbf{I}_K$, see (16). In this case, the matrices defined in (32) reduce to $\mathbf{\Gamma} = \mathbf{C}$, $\mathbf{\Phi} = \mathbf{I}_K$, and $\mathbf{M} = \mathbf{B}$. Thus, the filters $\mathbf{\Upsilon}(z)$ and $\mathbf{\Omega}(z)$ in (33) are of dimension $K \times K$ and are given by

$$\mathbf{\Upsilon}(z) = \mathbf{\Psi}^{-T}\left(\mathbf{C} + \mathbf{B}^T\mathbf{P}\mathbf{A}\right)(z\mathbf{I}_n - \mathbf{A})^{-1}\mathbf{B}$$
$$\mathbf{\Omega}(z) = \mathbf{\Psi} + \mathbf{\Upsilon}(z) \tag{38}$$

[13]$|\mathbb{U}|$ denotes the cardinality of $\mathbb{U}$.

where $\mathbf{\Psi} \in \mathbb{R}^{K\times K}$ is obtained from the factorization $\mathbf{\Psi}^T\mathbf{\Psi} = \mathbf{I}_K + \mathbf{B}^T\mathbf{P}\mathbf{B}$. As a consequence, the dynamics of the MHSBQ in Fig. 7 are governed by

$$\mathbf{u}(k) = \mathbf{\Psi}^{-1} q_{\widetilde{\mathbb{U}}}(\mathbf{c}(k))$$

where

$$\mathbf{c} \triangleq \mathbf{\Psi}^{-T}\big(\widetilde{\mathbf{W}}(z)\mathbf{H}(z)\mathbf{d} - (\widetilde{\mathbf{W}}(z) - \mathbf{\Psi}^T\mathbf{\Psi})\mathbf{u}\big),$$
$$\widetilde{\mathbf{W}}(z) \triangleq \mathbf{\Psi}^T\mathbf{\Psi} + \big(\mathbf{C} + \mathbf{B}^T\mathbf{P}\mathbf{A}\big)(z\mathbf{I}_n - \mathbf{A})^{-1}\mathbf{B}. \quad (39)$$

If we furthermore use no terminal state weighting, i.e., $\mathbf{P} = \mathbf{0}_n$, then $\mathbf{\Psi} = \mathbf{I}_K$, $\widetilde{\mathbb{U}} = \mathbb{U}$, and $\widetilde{\mathbf{W}}(z) = \mathbf{W}(z)$ so that the dynamics of the MHSBQ are described by

$$\mathbf{u}(k) = q_{\mathbb{U}}(\mathbf{c}(k))$$

with

$$\mathbf{c} = \mathbf{W}(z)\mathbf{H}(z)\mathbf{d} - (\mathbf{W}(z) - \mathbf{I}_K)\mathbf{u}.$$

On the other hand, the noise-shaping quantizer of Fig. 3 is characterized via

$$\mathbf{u}(k) = q_{\mathbb{U}}(\mathbf{b}(k))$$

where

$$\mathbf{b} \triangleq \mathbf{G}^{-1}(z)\mathbf{v} - (\mathbf{G}^{-1}(z) - \mathbf{I}_K)\mathbf{u}.$$

Thus, the two schemes are algebraically equivalent, if we set

$$\mathbf{W}(z) = \mathbf{G}^{-1}(z) \quad \text{and} \quad \mathbf{H}(z) = \mathbf{E}(z). \quad (40)$$

With respect to the signal predictive quantizer of Fig. 4, direct algebraic manipulation yields that equivalence is obtained if we set

$$\mathbf{W}(z) = \mathbf{G}^{-1}(z) \quad \text{and} \quad \mathbf{H}(z) = \mathbf{G}(z)\mathbf{E}(z).$$

We can therefore conclude that the subband MHSBQ is a generalization of both the noise-shaping quantizer, and the signal predictive quantizer proposed in [8]. In particular, the MHSBQ extends the linear feedback subband quantizers in [8] in two ways.

1) It allows for multistep optimality by choosing $N > 1$.
2) Stability concepts can be directly included into the design via the final state weighting matrix $\mathbf{P}$.

As documented in the sequel, these two aspects can be used to give enhanced performance of the MHSBQ, when compared to [8].

Remark 4 (Resultant Design Procedure): It is interesting to note that the relationships established above suggest a design procedure for the filters $\mathbf{W}(z)$ and $\mathbf{H}(z)$ which can be used in MHSBQs with *any* horizon $N \geq 1$ and *any* final state weighting matrix $\mathbf{P}$. Indeed, given a design for $\mathbf{G}(z)$ obtained, for example, via the technique in [8], the filters $\mathbf{W}(z)$ and $\mathbf{H}(z)$ can be synthesized according to (40). We note, however, that, whilst this is certainly possible, the MHSBQs so obtained will, in general, give worse performance than those which are based on filters $\mathbf{W}(z)$ and $\mathbf{H}(z)$ designed via (28). This will be illustrated in a simple example in Section V-C. △

Remark 5 (Stable Linear Feedback Subband Quantization): If $0 \in \mathbb{U}_i$, $\forall i \in \{1, 2, \ldots, K\}$, and if $\mathbf{P}$ in (39) is chosen to satisfy (23), then Theorem 1 states that the resultant MHSBQ with horizon $N = 1$ will have no idle tones. This subband quantization architecture can be regarded as a *stabilized linear feedback quantizer*. Note that for $N = 1$ the cardinality of the image set of the VQ underlying the MHSBQ, namely $q_{\widetilde{\mathbb{U}}}(\cdot)$, is equal to the sum of the cardinalities of the image sets of the K scalar quantizers used in the linear feedback quantizers in [8], i.e., of $q_{\mathbb{U}_i}(\cdot)$, $i \in \{1, 2, \ldots, K\}$. Thus, idle tone suppression can be guaranteed at the expense of only a small increase in on-line computational effort/circuit complexity. △

C. Example: Two-Channel Haar FB

As a simple example, adopted from [8], consider a two-channel oversampled FB with $L = 1$, corresponding to an oversampling factor of $r = 2$, see (4). The analysis FB is formed by the *Haar filters*

$$E_1(z) = \frac{1}{\sqrt{2}}(1 + z^{-1}), \quad E_2(z) = \frac{1}{\sqrt{2}}(1 - z^{-1})$$

and the synthesis FB (corresponding to the para-pseudoinverse of the analysis FB) is characterized by

$$R_1(z) = \frac{1}{2\sqrt{2}}(1 + z), \quad R_2(z) = \frac{1}{2\sqrt{2}}(1 - z).$$

This choice corresponds to the polyphase description

$$\mathbf{E}(z) = \frac{1}{\sqrt{2}}\begin{bmatrix} 1 + z^{-1} \\ 1 - z^{-1} \end{bmatrix}, \quad \mathbf{R}(z) = \frac{1}{2\sqrt{2}}\begin{bmatrix} 1 + z & 1 - z \end{bmatrix}$$

and, thus, satisfies the perfect reconstruction condition (8).

We consider four situations: First, we design the MHSBQ following (28), with $\delta = 1$

$$\mathbf{H}(z) = \frac{1}{\sqrt{2}}\begin{bmatrix} 1 + z^{-1} \\ 1 - z^{-1} \end{bmatrix}$$
$$\mathbf{W}(z) = \frac{1}{2\sqrt{2}}\begin{bmatrix} 1 + z^{-1} & -1 + z^{-1} \end{bmatrix}. \quad (41)$$

A state-space description of the filter $\mathbf{W}(z)$ in (41) is given by (16) where $n = 1$ and

$$\mathbf{A} = \mathbf{0}_1,\ \mathbf{B} = \frac{1}{2\sqrt{2}}\begin{bmatrix} 1 & 1 \end{bmatrix}$$
$$\mathbf{C} = \mathbf{I}_1,\ \mathbf{D} = \frac{1}{2\sqrt{2}}\begin{bmatrix} 1 & -1 \end{bmatrix}.$$

We set $\mathbf{P}$ as in Theorem 1, i.e., as the solution to (23), which here simply gives $\mathbf{P} = \mathbf{I}_1$. We also analyze the case of no final state weighting, i.e., $\mathbf{P} = \mathbf{0}_1$.

In a second setup, we utilize the noise-shaping filter of [8], namely

$$\mathbf{G}(z) = \mathbf{I}_2 - z^{-1}\begin{bmatrix} 0.5 & 0.5 \\ -0.5 & -0.5 \end{bmatrix}$$

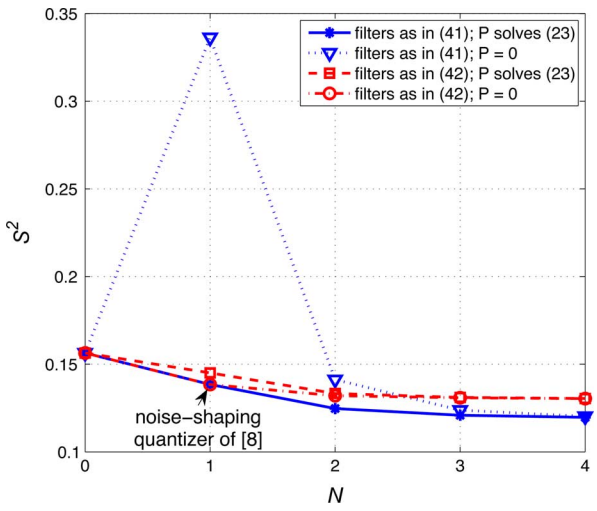

Fig. 8. Reconstruction error variance provided by the Haar FB with MHSBQ using the filters given in (41) (solid and dotted lines) and in (42) (dashed and dash-dotted lines). The noise-shaping quantizer of [8] corresponds to the MHSBQ designed according to (42) with $N = 1$ and $\mathbf{P} = \mathbf{0}_1$.

and compute $\mathbf{W}(z)$ and $\mathbf{H}(z)$ according to (40)

$$\mathbf{H}(z) = \frac{1}{\sqrt{2}}\begin{bmatrix} 1 + z^{-1} \\ 1 - z^{-1} \end{bmatrix}$$
$$\mathbf{W}(z) = \mathbf{G}^{-1}(z) = \begin{bmatrix} 1 + 0.5z^{-1} & 0.5z^{-1} \\ -0.5z^{-1} & 1 - 0.5z^{-1} \end{bmatrix}. \quad (42)$$

A state-space realization of $\mathbf{W}(z)$ in (42) is (16) with $n = 1$ and

$$\mathbf{A} = \mathbf{0}_1,\ \mathbf{B} = \frac{1}{\sqrt{2}}[1 \quad 1]$$
$$\mathbf{C} = \frac{1}{\sqrt{2}}\begin{bmatrix} 1 \\ -1 \end{bmatrix},\ \mathbf{D} = \mathbf{I}_2.$$

Again, we analyze two cases, namely no final state weighting, i.e., $\mathbf{P} = \mathbf{0}_1$, and $\mathbf{P}$ chosen according to (23), which, in this situation, gives $\mathbf{P} = \mathbf{I}_1$. It is worth noting that the noise-shaping quantizer of [8] is equivalent to the MHSBQ with design parameters $N = 1$, $\mathbf{P} = \mathbf{0}_1$, and $\mathbf{W}(z)$ and $\mathbf{H}(z)$ as in (42).

To compare the relative merits of these design choices, we fix the constraint sets according to $\mathbb{U}_1 = \mathbb{U}_2 = \{-1, 0, 1\}$, and use, as input signal y, $T_f = 1000$ samples of an i.i.d. real-valued Gaussian process having zero-mean and unit variance. Fig. 8 shows the values of the reconstruction error variance, defined as [14]

$$S^2 \triangleq \frac{1}{T_f}\sum_{\ell=0}^{T_f-1}(y(\ell) - \hat{y}(\ell))^2. \quad (43)$$

As can be seen from Fig. 8, performance improves in all four cases as the horizon N is increased beyond $N = 1$.[15] In particular, all MHSBQs with $\mathbf{P}$ chosen as in Theorem 1 and for horizon $N \geq 2$, outperform the noise-shaping subband quantizer proposed in [8]. Given that by setting the weighting filter $\mathbf{W}(z)$ as in (41) the MHSBQ aims at minimizing the reconstruction error $\mathbf{e_d}$, see (30), we observe in Fig. 8 that choosing $\mathbf{W}(z)$ as in (41) and $\mathbf{P}$ to solve (23) gives the best results.

[14]We average over 100 realizations of the input sequence.

[15]Here and in the sequel, $N = 0$ denotes direct quantization as in (11).

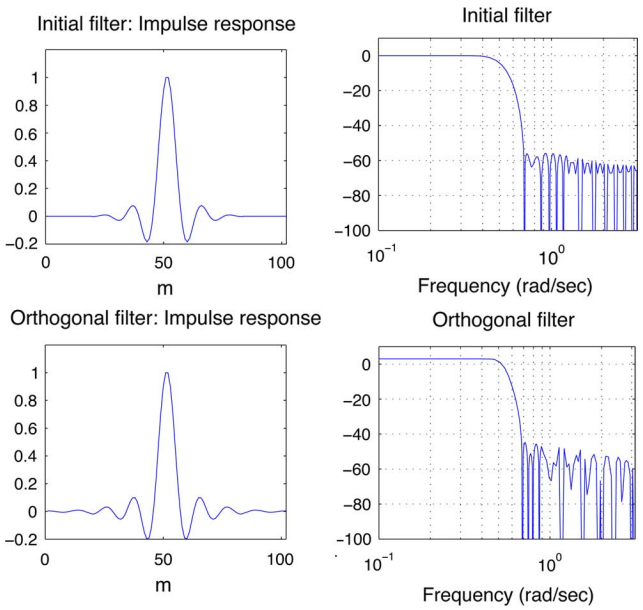

Fig. 9. Result of the orthogonalization procedure in [49]: Upper plots show impulse response (LHS) and magnitude of transfer function (RHS) of initial filter; lower plots show corresponding orthogonal filter leading to a paraunitary even-stacked CMFB.

The benefits of choosing $\mathbf{P}$ as in Theorem 1 are apparent when $\mathbf{W}(z)$ is chosen as in (41) and for horizon $N = 1$. Interestingly, in this specific example, with $\mathbf{W}(z)$ as in (42) and $N \in \{1, 2\}$, choosing $\mathbf{P} = \mathbf{0}_1$ gives better performance than using the value of $\mathbf{P}$ which solves (23).

VI. Design Study: Cosine-Modulated FBs (CMFBs)

CMFBs [44]–[47] have received significant attention as they can be designed with relative ease (all subband filters correspond to modulated versions of a single prototype filter) and allow for a computationally efficient implementation (based on the DCT). In the following, we investigate a six-channel ($K = 6$) *even-stacked CMFB* [47] with oversampling factor 3 (i.e., $L = 2$).[16] We utilize an FIR prototype filter of the form

$$H^p(z) = \sum_{m=0}^{L_h-1} h^p(m)z^{-m} \quad (44)$$

where L_h is even ($L_h = 102$), and which satisfies the linear phase property, i.e.

$$h^p(m) = h^p(L_h - 1 - m), \quad \forall m \in \{0, 1, \ldots, L_h - 1\}. \quad (45)$$

We design the prototype filter $H^p(z)$ by applying the orthogonalization method proposed in [49] to an initial lowpass filter (designed with bandwidth $1/K$). Fig. 9 shows the initial filter and the resulting orthogonal filter. As can be seen, the orthogonalized prototype filter $H^p(z)$ exhibits time- and frequency-characteristics that are similar to those of the original (nonorthogonal) filter. It is worth noting that the impulse response of $H^p(z)$ is negligible for $m \leq 0$ and for $m \geq 100$. The resulting analysis FB is paraunitary, see [47] and [49]. We can, therefore, synthesize a perfect reconstruction

[16]Even-stacked CMFBs possess the additional property of all subchannel filters being linear-phase, a property useful, for example, in image coding applications [48]. Further details on (oversampled) CMFBs can be found in [47].

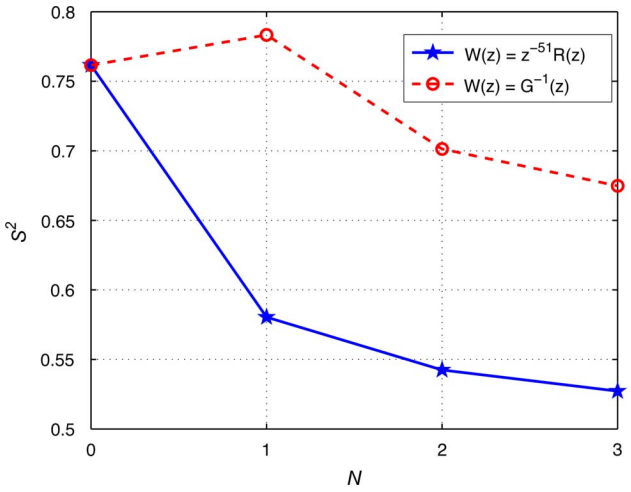

Fig. 10. Reconstruction error variance as a function of N, $\mathbf{P}$ solves (23).

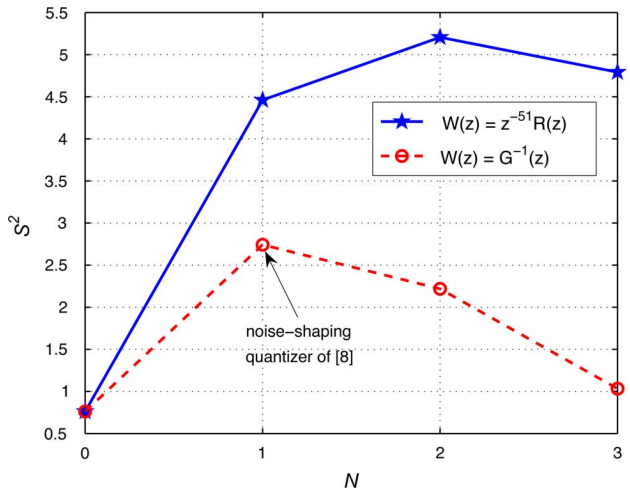

Fig. 11. Reconstruction error variance as a function of N, $\mathbf{P} = \mathbf{0}_n$.

FB, see Section II-C, by choosing the synthesis FB to be an even-stacked CMFB with prototype filter

$$F^p(z) = \sum_{m=-L_h+1}^{0} f^p(m) z^{-m}$$

where

$$f^p(m) = h^p(-m). \tag{46}$$

Simulations were carried out with binary sets $\mathcal{U}_i = \{-1, 1\}$, $\forall i \in \{1, 2, \ldots, 6\}$, and the input y was chosen as $T_f = 1000$ samples of an i.i.d. real valued Gaussian random process having zero-mean and variance 4.

The following design choices were considered: $\mathbf{H}(z) = \mathbf{E}(z)$ and $\mathbf{W}(z) = z^{-51}\mathbf{R}(z)$, see (28); and $\mathbf{H}(z) = \mathbf{E}(z)$ and $\mathbf{W}(z) = \mathbf{G}^{-1}(z)$, see (40).[17] Moreover, we investigated horizons $N \in \{0, 1, 2, 3\}$, final state weighting as in (23) as well as no final state weighting, i.e., $\mathbf{P} = \mathbf{0}_n$, where n is the order of the filters $\mathbf{W}(z)$ used in each case. Again, we point out that, as shown in Section V-B, the noise shaping structure investigated in [8] corresponds to the MHSBQ with design parameters $N = 1$, $\mathbf{P} = \mathbf{0}_n$, and $\mathbf{W}(z) = \mathbf{G}^{-1}(z)$.

Figs. 10 and 11 contain the sample reconstruction error variances obtained, see (43). It can be seen that the benefit of choosing $\mathbf{W}(z) = z^{-51}\mathbf{R}(z)$ and employing final state weighting according to (23) is remarkable. With these design parameters, larger horizons give better performance and also with a modest value of N, say $N = 2$, we obtain excellent results when compared to the designs where $\mathbf{P} = \mathbf{0}_n$. These observations are representative of many experiments that we have performed.

It is interesting to note that, as can be seen in Fig. 11, in the example at hand, all designs where $\mathbf{P} = \mathbf{0}_n$ give worse performance than direct quantization following (11) (which is here denoted as $N = 0$). We can therefore conclude that final state weighting is crucial to achieve good performance.[18] Finally, comparing the case $N = 2$ and $\mathbf{P}$ solving (23) to the noise-shaping quantizer in [8] (i.e., $N = 1$ and $\mathbf{P} = \mathbf{0}_n$), we can see that MHSBQ with final state weighting leads to a reduction in reconstruction MSE of more than 80%.

VII. Conclusion

We proposed a novel method for quantizing filter bank frame expansions. Our strategy minimizes a filtered distortion sequence in a moving horizon fashion. The structure described in this paper includes the linear feedback subband quantizers proposed in [8] as special cases. More precisely, while linear feedback quantizers are only one-step optimal, the quantizer proposed in this paper is multistep optimal. The new approach leads to enhanced performance, compared to the methods described in [8], and offers the possibility of guaranteeing the absence of idle-tones. Open problems include characterizing the MSE of the MHSBQ as a function of the oversampling factor, further establishing the relationship to [20]–[24], and extending the MHSBQ to general frame expansions.

Appendix
Proof of Theorem 1

The proof uses the sequence of optimal costs defined as $V_N^\star(k) \triangleq V_N(\vec{\mathbf{u}}^\star(k); \mathbf{x}(k))$, $k \in \mathbb{Z}$, with $\vec{\mathbf{u}}^\star(k)$ and $\mathbf{x}(k)$ defined in (17) and (22), respectively.

Suppose that, at time k, an optimal sequence

$$\vec{\mathbf{u}}^\star(k) = \begin{bmatrix} \mathbf{u}^\star(k) \\ \mathbf{u}_{k+1} \\ \vdots \\ \mathbf{u}_{k+N-1} \end{bmatrix} \tag{47}$$

[17]Here, $\mathbf{G}(z)$ was chosen as an FIR filter of order 2, designed according to the procedure proposed in [8].

[18]Note that in the present case $0 \notin \mathcal{U}_i$. Thus, we cannot guarantee absence of idle tones.

has been found. Thus, at sample $k+1$, it follows from (27) that $\mathbf{x}(k+1) = \mathbf{A}\mathbf{x}(k) + \mathbf{B}(\mathbf{a}(k) - \mathbf{u}^\star(k))$ with $\mathbf{u}^\star(k)$ given by (26). Next, consider the related sequence

$$\mathbf{u}^s = \begin{bmatrix} \mathbf{u}_{k+1} \\ \mathbf{u}_{k+2} \\ \vdots \\ \mathbf{u}_{k+N-1} \\ \mathbf{a}(k+N) \end{bmatrix} \in \mathbb{U}^N. \tag{48}$$

Direct calculation then yields

$$\begin{aligned} &V_N(\mathbf{u}^s; \mathbf{x}(k+1)) \\ &\quad = V_N^\star(k) + ||\mathbf{A}\mathbf{x}(k+N)||_{\mathbf{P}}^2 \\ &\qquad - ||\mathbf{x}(k+N)||_{\mathbf{P}}^2 + ||\mathbf{e}_f(k+N)||^2 - ||\mathbf{e}_f(k)||^2 \\ &\quad = V_N^\star(k) + ||\mathbf{A}\mathbf{x}(k+N)||_{\mathbf{P}}^2 - ||\mathbf{x}(k+N)||_{\mathbf{P}}^2 \\ &\qquad + ||\mathbf{C}\mathbf{x}(k+N)||^2 - ||\mathbf{e}_f(k)||^2 \end{aligned}$$

where we have used (17). Since $V_N^\star(k+1)$ corresponds to the optimal choice $\vec{\mathbf{u}}^\star(k+1)$, we have that $V_N^\star(k+1) \leq V_N(\mathbf{u}^s; \mathbf{x}(k+1))$. Hence, using (23), we obtain

$$\begin{aligned} &V_N^\star(k+1) \\ &\quad \leq V_N^\star(k) + ||\mathbf{A}\mathbf{x}(k+N)||_{\mathbf{P}}^2 \\ &\qquad - ||\mathbf{x}(k+N)||_{\mathbf{P}}^2 + ||\mathbf{C}\mathbf{x}(k+N)||^2 \\ &\qquad - ||\mathbf{e}_f(k)||^2 \\ &\quad = V_N^\star(k) + ||\mathbf{x}(k+N)||_{\mathbf{A}^T\mathbf{P}\mathbf{A}-\mathbf{P}+\mathbf{C}^T\mathbf{C}}^2 \\ &\qquad - ||\mathbf{e}_f(k)||^2 \\ &\quad = V_N^\star(k) - ||\mathbf{e}_f(k)||^2 \leq V_N^\star(k) \end{aligned} \tag{49}$$

i.e., the sequence $V_N^\star(k)$ is nonincreasing. Since $V_N^\star(k) \geq 0$, $\forall k \in \mathbb{Z}$, it follows that the sequence $V_N^\star(k)$ is convergent, thus, $\lim_{k\to\infty} V_N^\star(k)$ exists.

As a consequence of (49), we also have

$$V_N^\star(k+1) - V_N^\star(k) \leq -||\mathbf{e}_f(k)||^2 \leq 0. \tag{50}$$

Since $V_N^\star(k)$ is convergent, it holds that

$$\lim_{k\to\infty} \left(V_N^\star(k+1) - V_N^\star(k)\right) = 0$$

so that, by using (50), we obtain $\lim_{k\to\infty} ||\mathbf{e}_f(k)||^2 = 0$ and, thus, $\lim_{k\to\infty} \mathbf{e}_f(k) = \mathbf{0}$. ■

REFERENCES

[1] R. E. Crochiere and L. R. Rabiner, *Multirate Digital Signal Processing*. Englewood Cliffs, NJ: Prentice-Hall, 1983.

[2] M. Vetterli and J. Kovačević, *Wavelets and Subband Coding*. Englewood Cliffs, NJ: Prentice-Hall, 1995.

[3] P. P. Vaidyanathan, *Multirate Systems and Filter Banks*. Englewood Cliffs, NJ: Prentice-Hall, 1993.

[4] N. Fliege, *Multirate Digital Signal Processing: Multirate Systems, Filter Banks, Wavelets*. New York: Wiley, 1994.

[5] G. Strang and T. Nguyen, *Wavelets and Filter Banks*. Wellesley, MA: Wellesley-Cambridge, 1996.

[6] *Collected Papers on Digital Audio Bit-Rate Reduction*, N. Gilchrist and C. Grewin, Eds. New York: Audio Eng. Soc., 1996.

[7] Z. Cvetković and J. D. Johnson, "Nonuniform oversampled filter banks for audio signal processing," *IEEE Trans. Speech Audio Process.*, vol. 11, pp. 393–399, Sep. 2003.

[8] H. Bölcskei and F. Hlawatsch, "Noise reduction in oversampled filter banks using predictive quantization," *IEEE Trans. Inf. Theory*, vol. 47, pp. 155–172, Jan. 2001.

[9] H. Vikalo, B. Hassibi, A. T. Erdogan, and T. Kailath, "On robust signal reconstruction in noisy filter banks," *Signal Process.*, vol. 85, no. 1, pp. 1–14, Jan. 2005.

[10] Y. -M. Cheng, B. -S. Chen, and L. -M. Chen, "Minimax deconvolution design of multirate systems with channel noises: A unified approach," *IEEE Trans. Signal Process.*, vol. 47, pp. 3145–3149, Nov. 1999.

[11] A. Makur and M. Arunkumar, "Minimization of quantization noise amplification in biorthogonal subband coders," *IEEE Trans. Circuits Syst. I*, vol. 51, pp. 2088–2097, Oct. 2004.

[12] S. K. Tewksbury and R. W. Hallock, "Oversampled, linear predictive and noise-shaping coders of order $N > 1$," *IEEE Trans. Circuits Syst.*, vol. 25, pp. 436–447, Jul. 1978.

[13] *Delta-Sigma Data Converters: Theory, Design and Simulation*, S. R. Norsworthy, R. Schreier, and G. C. Temes, Eds. Piscataway, NJ: IEEE, 1997.

[14] D. E. Quevedo, G. C. Goodwin, and J. A. De Doná, "Finite constraint set receding horizon quadratic control," *Int. J. Robust Nonlin. Contr.*, vol. 14, no. 4, pp. 355–377, Mar. 2004.

[15] G. C. Goodwin, D. E. Quevedo, and D. McGrath, "Moving-horizon optimal quantizer for audio signals," *J. Audio Eng. Soc.*, vol. 51, no. 3, pp. 138–149, Mar. 2003.

[16] D. E. Quevedo and G. C. Goodwin, "Multistep optimal analog-to-digital conversion," *IEEE Trans. Circuits Syst. I*, vol. 52, pp. 503–515, Mar. 2005.

[17] D. E. Quevedo and G. C. Goodwin, "Moving horizon design of discrete coefficient FIR filters," *IEEE Trans. Signal Process.*, vol. 53, pp. 2262–2267, Jun. 2005.

[18] D. E. Quevedo, G. C. Goodwin, and J. A. De Doná, "Multistep detector for linear ISI-channels incorporating degrees of belief in past estimates," *IEEE Trans. Commun.*, vol. 55, pp. 2092–2103, Nov. 2007.

[19] C. S. Güntürk, T. Nguyen, A. M. Powell, and O. Yilmaz, "Coarsely Quantized Redundant Representations of Signals, Final Workshop Report," Int. Res. Station for Math. Innovat. Disc., Banff, 2006.

[20] I. Daubechies and R. DeVore, "Approximating a bandlimited function using very coarsely quantized data: A family of stable sigma-delta modulators of arbitrary order," *Ann. Math.*, vol. 158, no. 2, pp. 679–710, Sep. 2003.

[21] J. J. Benedetto, A. M. Powell, and O. Yilmaz, "Sigma-delta $(\Sigma\Delta)$ quantization and finite frames," *IEEE Trans. Inf. Theory*, vol. 52, pp. 1990–2005, May 2006.

[22] J. J. Benedetto, A. M. Powell, and O. Yilmaz, "Second-order sigma-delta $(\Sigma\Delta)$ quantization of finite frame expansions," *Appl. Comput. Harmon. Anal.*, vol. 20, no. 1, pp. 126–148, Jan. 2006.

[23] I. Daubechies, R. DeVore, C. S. Güntürk, and V. A. Vaishampayan, "A/D conversion with imperfect quantizers," *IEEE Trans. Inf. Theory*, vol. 52, pp. 874–885, Mar. 2006.

[24] C. S. Güntürk and N. T. Thao, "Refined error analysis in second-order $\Sigma\Delta$ modulation with constant inputs," *IEEE Trans. Inf. Theory*, vol. 50, pp. 839–860, May 2004.

[25] M. S. Derpich, E. I. Silva, D. E. Quevedo, and G. C. Goodwin, "On optimal perfect reconstruction feedback quantizers," *IEEE Trans. Signal Process.*, vol. 56, pp. 3871–3890, Aug. 2008.

[26] Z. Cvetković and M. Vetterli, "Oversampled filter banks," *IEEE Trans. Signal Process.*, vol. 46, pp. 1245–1255, May 1998.

[27] H. Bölcskei, F. Hlawatsch, and H. G. Feichtinger, "Frame-theoretic analysis of oversampled filter banks," *IEEE Trans. Signal Process.*, vol. 46, pp. 3256–3268, Dec. 1998.

[28] B. -S. Chen, C. -W. Lin, and Y. -L. Chen, "Optimal signal reconstruction in noisy filter bank systems: Multirate Kalman synthesis filtering approach," *IEEE Trans. Signal Process.*, vol. 43, pp. 2496–2504, Nov. 1995.

[29] D. Marco and D. L. Neuhoff, "The validity of the additive noise model for uniform scalar quantizers," *IEEE Trans. Inf. Theory*, vol. 51, pp. 1739–1755, May 2005.

[30] P. Westerink, J. Biemond, and D. E. Boekee, "Scalar quantization error analysis for image subband coding using QMF's," *IEEE Trans. Signal Process.*, vol. 40, pp. 421–428, Feb. 1992.

[31] O. Feely, "Nonlinear dynamics of discrete-time circuits: A survey," *Int. J. Circuit Theory Appl.*, vol. 35, no. 5-6, pp. 515–531, Sep.-Dec. 2007.

[32] R. A. Haddad and K. Park, "Modeling, analysis, and optimum design of quantized M-band filter banks," *IEEE Trans. Signal Process.*, vol. 43, pp. 2540–2549, Nov. 1995.

[33] N. Jayant, J. Johnston, and R. Safranek, "Signal compression based on models of human perception," *Proc. IEEE*, vol. 81, pp. 1385–1421, Oct. 1993.
[34] A. Eshraghi and T. S. Fiez, "A comparative analysis of parallel delta-sigma ADC converter architectures," *IEEE Trans. Circuits Syst. I*, vol. 51, pp. 450–458, Mar. 2004.
[35] D. Q. Mayne, J. B. Rawlings, C. V. Rao, and P. O. M. Scokaert, "Constrained model predictive control: Optimality and stability," *Automatica*, vol. 36, no. 6, pp. 789–814, Jun. 2000.
[36] G. C. Goodwin, M. M. Serón, and J. A. De Doná, *Constrained Control and Estimation—An Optimization Perspective*. London, U.K.: Springer-Verlag, 2005.
[37] T. Kailath, *Linear systems*. Englewood Cliffs, N.J: Prentice-Hall, 1980.
[38] B. D. O. Anderson and J. Moore, *Optimal filtering*. Englewood Cliffs, NJ: Prentice-Hall, 1979.
[39] Z. Pan, K. Kotani, and T. Ohmi, "A unified projection method for fast search of vector quantization," *IEEE Signal Process. Lett.*, vol. 11, pp. 637–640, Jul. 2004.
[40] J. -S. Pan, Z. -M. Lu, and S. -H. Sun, "An efficient encoding algorithm for vector quantization based on subvector technique," *IEEE Trans. Image Process.*, vol. 12, pp. 265–270, Mar. 2003.
[41] G. D. Forney, "Maximum likelihood sequence estimation of digital sequences in the presence of intersymbol interference," *IEEE Trans. Inf. Theory*, vol. 18, pp. 363–378, May 1972.
[42] D. F. Delchamps, "Nonlinear dynamics of oversampling A-to-D converters," in *Proc. IEEE Conf. Decision Contr.*, Dec. 1993, vol. 1, pp. 480–485.
[43] P. J. Ramadge, "On the periodicity of symbolic observations of piecewise smooth discrete-time systems," *IEEE Trans. Autom. Control*, vol. 35, pp. 807–813, Jul. 1990.
[44] Y.-P. Lin and P. P. Vaidyanathan, "Linear phase cosine modulated maximally decimated filter banks with perfect reconstruction," *IEEE Trans. Signal Process.*, vol. 42, pp. 2525–2539, Nov. 1995.
[45] R. D. Koilpillai and P. P. Vaidyanathan, "Cosine-modulated FIR filter banks satisfying perfect reconstruction," *IEEE Trans. Signal Process.*, vol. 40, pp. 770–783, Apr. 1992.
[46] W.-S. Lu, T. Saramäki, and R. Bregović, "Design of practically perfect-reconstruction cosine-modulated filter banks: A second-order cone programming approach," *IEEE Trans. Circuits Syst. I*, vol. 51, pp. 552–563, Mar. 2004.
[47] H. Bölcskei and F. Hlawatsch, "Oversampled cosine modulated filter banks with perfect reconstruction," *IEEE Trans. Circuits Syst. II*, vol. 45, pp. 1057–1071, Aug. 1998.
[48] J. L. Mannos and D. J. Sakrison, "The effect of a visual fidelity criterion on the encoding of images," *IEEE Trans. Inf. Theory*, vol. 20, pp. 525–536, Jul. 1974.
[49] H. Bölcskei, P. Duhamel, and R. Hleiss, "Orthogonalization of OFDM/OQAM pulse shaping filters using the discrete Zak transform," *Signal Process.*, vol. 83, no. 7, pp. 1379–1391, Jul. 2003.

Daniel E. Quevedo (M'05) received the Ingeniero Civil Electrónico and Magister en Ingeniería Electrónica degrees from the Universidad Técnica Federico Santa María, Valparaíso, Chile, in 2000. He received the Ph.D. degree from The University of Newcastle, Australia, in 2005.

He is an Australian Research Fellow at the University of Newcastle. He has lectured at the Universidad Técnica Federico Santa María and The University of Newcastle. He also has working experience with the VEW Energie AG, Dortmund, Germany, and with the Cerro Tololo Inter-American Observatory, La Serena, Chile. His research interests cover several areas of automatic control, signal processing, and communications.

Dr. Quevedo was supported by a full scholarship from the alumni association during his time with the Universidad Técnica Federico Santa María and received several university-wide prizes upon graduating. He received the IEEE Conference on Decision and Control Best Student Paper Award in 2003 and was also a finalist in 2002.

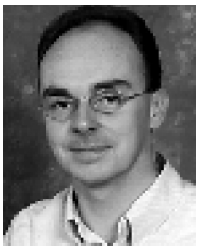

Helmut Bölcskei (F'09) was born in Mödling, Austria, on May 29, 1970. He received the Dipl.-Ing. and Dr. techn. degrees in electrical engineering from Vienna University of Technology, Vienna, Austria, in 1994 and 1997, respectively.

In 1998, he was with Vienna University of Technology. From 1999 to 2001 he was a Postdoctoral Researcher in the Information Systems Laboratory, Department of Electrical Engineering, Stanford University, Stanford, CA. He was on the founding team of Iospan Wireless Inc., a Silicon Valley-based startup company (acquired by Intel Corporation in 2002) specialized in multiple-input multiple-output (MIMO) wireless systems for high-speed Internet access. From 2001 to 2002, he was an Assistant Professor of Electrical Engineering with the University of Illinois at Urbana-Champaign. He has been with ETH Zurich, Switzerland, since 2002, where he is a Professor of Communication Theory. He was a visiting researcher with Philips Research Laboratories Eindhoven, The Netherlands, ENST Paris, France, and the Heinrich Hertz Institute Berlin, Germany. His research interests include information theory, signal processing, and harmonic analysis.

Dr. Bölcskei received the 2001 IEEE Signal Processing Society Young Author Best Paper Award, the 2006 IEEE Communications Society Leonard G. Abraham Best Paper Award, the ETH "Golden Owl" Teaching Award, and was an Erwin Schrödinger Fellow (1999–2001) of the Austrian National Science Foundation (FWF). He was a plenary speaker at several IEEE conferences and served as an Associate Editor of the IEEE TRANSACTIONS ON SIGNAL PROCESSING, the IEEE TRANSACTIONS ON WIRELESS COMMUNICATIONS, and the EURASIP *Journal on Applied Signal Processing*. He is currently on the editorial board of *Foundations and Trends in Networking*, serves as an Associate Editor for the IEEE TRANSACTIONS ON INFORMATION THEORY and is TPC co-chair of the 2008 IEEE International Symposium on Information Theory.

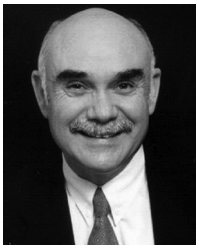

Graham C. Goodwin (F'86) received the B.Sc. (physics), B.E. (electrical engineering), and the Ph.D. degree from the University of New South Wales.

He is currently Professor of Electrical Engineering at the University of Newcastle, Australia, and holds Honorary Doctorates from Lund Institute of Technology, Sweden, and the Technion, Israel. He is the coauthor of eight books, four edited volumes, and many technical papers.

Dr. Goodwin is the recipient of the Control Systems Society 1999 Hendrik Bode Lecture Prize, a Best Paper award from the IEEE TRANSACTIONS ON AUTOMATIC CONTROL, a Best Paper award by the *Asian Journal of Control*, and two Best Engineering Text Book awards from the International Federation of Automatic Control. He is an Honorary Fellow of the Institute of Engineers, Australia; a Fellow of the Australian Academy of Science; a Fellow of the Australian Academy of Technology, Science and Engineering; a Member of the International Statistical Institute; a Fellow of the Royal Society, London, and a Foreign Member of the Royal Swedish Academy of Sciences.